Gas/Water Flow in Porous Media in the Presence of Adsorbed Polymer: Experimental Study on Non-Darcy Effects

V. Blanchard, Didier Lasseux, H. Bertin, T. Pichery, G. Chauveteau, R. Tabary, A. Zaitoun

SPE Reservoir Evaluation and Engineering Journal, 2007, **10**(4), 423-431, doi: 10.2118/99711-PA

Gas/Water Flow in Porous Media in the Presence of Adsorbed Polymer: Experimental Study on Non-Darcy Effects

V. Blanchard, D. Lasseux, SPE, and **H. Bertin,** SPE, University of Bordeaux; **T. Pichery,** Gaz de France; and **G. Chauveteau, R. Tabary,** SPE, and **A. Zaitoun,** SPE, Institut Français du Pétrole

Summary

The objective of this paper is to report some experimental investigations on the effect of polymer adsorption on gas/water flow in non-Darcy regimes in homogeneous porous media, in contrast to previously available analyses focused mainly on the Darcy regime. Our investigation concentrates on gas flow either at low mean pressure, when Klinkenberg effects (or gas slippage) must be considered, or at high flow rates, when inertial effects are significant.

The experimental study reported here consists of water and nitrogen injections into various silicon carbide model granular packs having different permeabilities. Experiments are carried out at different water saturations before and after polymer adsorption over flow regimes ranging from slip flow to inertial flow. In good agreement with previous works, in the Darcy regime, we observe an increase in irreducible water saturation and a strong reduction in the relative permeability to water, while the relative permeability to gas is slightly affected. At low mean pressure in the gas phase, the magnitude of the Klinkenberg effect is found to increase with water saturation in the absence of polymer, whereas for the same water saturation, the presence of an adsorbed polymer layer reduces this effect. In the inertial regime, a reduction of inertial effects is observed when gas is injected after polymer adsorption, taking into account water-saturation and permeability modifications. Experimental data are discussed according to hypotheses put forth to explain these effects. Consequences for practical use are also put under prospect.

Introduction

Water/oil or water/gas flows in porous media are strongly modified in the presence of an adsorbed polymer layer on the pore surface. Several studies, performed in the Darcy regime, showed a phenomenon of disproportionate permeability reduction (DPR). The relative permeability to water (k_{rw}) is reduced more than the relative permeability to gas (k_{rg}) or to oil (k_{ro}). Although this effect was observed over most of the water-soluble polymer/weak gel systems and rock materials, the origin of this effect is still controversial in the literature. Several physical processes have been put forth to explain the selective action of the polymer.

- Mennella et al. (1998) studied water/oil flows in the presence of an adsorbed polymer layer in random packs of monodisperse spheres. They concluded that the DPR was caused by a swelling/shrinking effect depending on the kind of fluid flowing throughout the packs. They also explained the DPR by pore-scale topological modification (pore-size reduction). Similar studies (Dawe and Zhang 1994; Sparlin and Hagen 1984) were carried out on different systems such as micromodels.
- Some authors (White et al. 1973; Schneider and Owens 1982; Nilsson et al. 1998) have interpreted the effect of polymer by assuming that a porous medium is composed of separate oil/water pore networks. With this representation, the DPR can be explained by the fact that water permeability is affected by the hydrosoluble polymer present in the pore network occupied by water, while oil permeability is not.
- Many studies attributed the DPR to a wall effect (Zaitoun and Kohler 1988, 2000; Barreau 1996; Zaitoun et al. 1998), which decreases the pore section accessible to water. The physical origin of this mechanism is adsorption—almost irreversible—on the solid surface. An adsorbed polymer layer on pore walls induces steric hindrance, lubrication effects, and wettability modification, all of which are in favor of a stronger reduction of water permeability than of oil permeability. The physical relevance of this mechanism was tested on numerical simulations at the pore scale (Barreau et al. 1997).
- Liang and Seright (2000), following Nilsson et al. (1998), proposed to complete the explanation of DPR by a "gel-droplet" model. In this scenario, gel droplets formed in pore bodies cause a higher pressure drop at the pore throat in the wetting phase than in the nonwetting one.

These reported studies mainly have been dedicated to the polymer action on oil/water systems, and much less attention has been paid to gas/water flow. However, all available results in this last configuration lead to the same behavior, and the same type of physical explanation (wall effect) was proposed (Zaitoun and Kohler 1989; Zaitoun et al. 1991).

If published results dealing with the effect of polymer on permeability reduction observed in the Darcy regime are quite numerous, very little work has been dedicated to the non-Darcy regimes. Elmkies et al. (2002) reported laboratory experimental data showing that adsorbed polymer on natural porous-media cores decreases the inertial effects during gas flow.

In this paper, we focus our attention on the influence of adsorbed polymer on gas/water core flow in non-Darcy regimes. Gas injection was performed on unconsolidated cores having different permeabilities, at different water saturations, before and after polymer treatment, and at low mean pressure to investigate Klinkenberg effects, as well as at high flow rates, when inertial effects become important.

Models and Test Equipment

Porous Media. Cores were made of silicon carbide (SiC) powders, which are commercially available in a wide range of particle sizes with a relatively narrow distribution. Although plugging and packing difficulties may occur while using SiC powder, this choice was motivated by the fact that surface properties of this material are well understood (Médout-Marère et al. 2000), as well as porosity and permeability of SiC granular packs (Chauveteau et al. 1996.

In the present work, we used SiC with a mean grain size of $d_g = 30$ μm for the study of the Klinkenberg effect and $d_g = 50$ μm for the study of inertial effect.

Fluids. Water phases were brines ([KI] = 5 or 10 g/L), with sodium azide ([NaN_3] = 0.4 g/L) used as a bactericide to prevent polymer degradation. Brine was filtered through 0.22 μm Millipore* membranes. Potassium iodide was used as a tracer for dispersion experiments and to improve saturation-measurement ac-

* Mark of Millipore S.A.S., Molsheim Cedex, France.

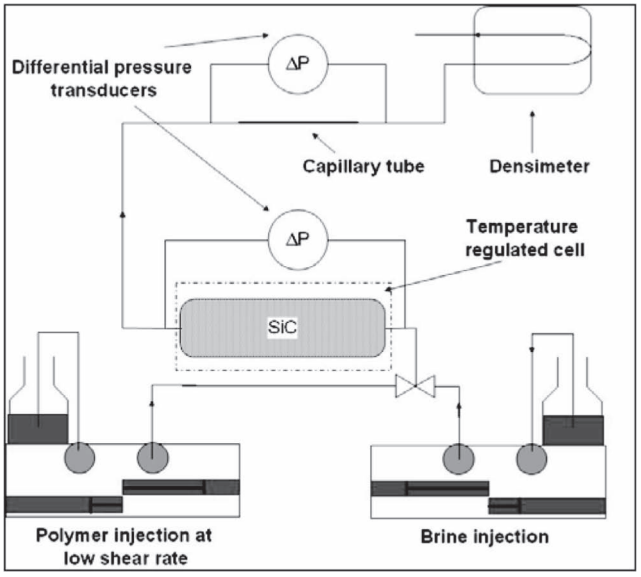

Fig. 1—Coreflood test equipment for polymer injection.

curacy by gamma ray attenuation (Nicholls and Heaviside 1988). The gas phase was dry pure nitrogen.

Polymer Solution. We used a nonionic polyacrylamide (PAM from Floerger), available in powder form with a molecular weight of 9 million dalton. The solution was prepared from slow addition of the polymer powder into the brine ([KI] = 5 g/L) in a vortex created by magnetic stirring. After complete dissolution of the powder, the solution was filtered with a set of 8-, 3-, and 1.2-μm Millipore membranes to remove microgels (Broseta et al. 1995). The final solution concentration, measured by total organic carbon analysis, is approximately 1,000 ppm.

Viscosity of the polymer solution was measured for a wide range of shear rates with a Contraves LS 30 Couette viscometer.

Brine and Polymer Injection. Polymer injection was performed using the coreflood test equipment represented schematically in **Fig. 1.** Estimation of the polymer adsorption requires the use of a salt dispersion front. To do so, a brine solution ([KI] = 5 g/L) was first injected into the core, initially saturated by a more-concentrated brine ([KI] = 10 g/L). The dispersion front was recorded by measuring the time evolution of the salt concentration of effluents at the outlet of the core using a densimeter. In a second step, the polymer solution was injected at a constant flow rate, ensuring the Newtonian behavior of the polymer solution, while the core and polymer solution were maintained at a constant temperature (T = 30°C). For practical reasons, dispersion-front experiments and polymer injections were performed on horizontally positioned cores, as indicated in Fig. 1. The core position is of no importance because in these steps of the experiment, gravity has no impact at the core-diameter scale because no significant density contrast (0.4%) exists between the fluid injected and that present in the core. Pressure drop was measured between the core inlet and outlet as well as between extremities of a capillary tube placed at the core outlet using two differential pressure transducers. The resulting permeability reduction to fluid i ($i = g$ or w), R_{ki}, caused by polymer adsorption was estimated by

$$R_{ki} = \frac{\Delta P_i^{(2)}}{\Delta P_i^{(1)}}, \quad \ldots\ldots (1)$$

where $\Delta P_i^{(1)}$ and $\Delta P_i^{(2)}$ are the pressure drop between core edges obtained at the same flow rate of fluid i before and after polymer adsorption, respectively.

Klinkenberg Effects. ***Physical Model.*** Our experiments were performed in absence or at a stationary water saturation S_w. Because of the absence of local water flux within the core (see description of experiments below), the problem can be treated as one-phase (gas) flow. Consequently, the one-phase 1D integrated form of Darcy's law can be used to interpret gas flow at the core scale, assuming constant temperature and considering the gas as ideal. In fact, the classical 1D local form of Darcy's law is

$$\frac{Q}{S}\,\mathrm{d}x = -\frac{k_{gl}}{\mu}\,\mathrm{d}P, \quad \ldots\ldots (2)$$

where μ is the gas dynamic viscosity, Q is the local volume flow rate, S is the porous-medium section, and k_{gl} is the apparent local gas permeability, while dP is the gas pressure drop over dx. Because of Klinkenberg effects, k_{gl} depends on gas pressure and can be expressed as (Klinkenberg 1941)

$$k_{gl} = k_g^{(\infty)}\left(1 + \frac{b}{P}\right), \quad \ldots\ldots (3)$$

where b is the Klinkenberg constant, while $k_g^{(\infty)}$ is the permeability to gas corrected by the Klinkenberg effect (i.e., the intrinsic permeability if $S_w = 0$ or the effective permeability at S_w otherwise). The momentum conservation equation (Eq. 2) must be associated to the local mass-conservation equation:

$$\frac{\mathrm{d}(\rho Q)}{\mathrm{d}x} = 0, \quad \ldots\ldots (4)$$

along with the ideal-gas law:

$$\rho = \frac{M}{RT}P. \quad \ldots\ldots (5)$$

In this last relation, R is the ideal-gas constant (R = 8.314 J.mol^{-1}.K^{-1}) and M is the molar mass of the gas, whereas ρ and T are its density and temperature, respectively. When Eq. 2 is multiplied by ρ and integrated between the core inlet ($x = 0$, pressure P_1, volume flow rate Q_1) and outlet ($x = L$, pressure P_2), one gets

$$\frac{P_1 Q_1}{S}L = \frac{k_g^{(\infty)}}{\mu}\left[\frac{1}{2}(P_1^2 - P_2^2) + b(P_1 - P_2)\right]. \quad \ldots\ldots (6)$$

To arrive at this result, we have used the ideal-gas law (Eq. 5) and the mass conservation in Eq. 4. Rearranging Eq. 6 leads to

$$\frac{\mu L Q_1 P_1}{S\Delta P} = k_g^{(\infty)}(P_m + b), \quad \ldots\ldots (7)$$

or, equivalently,

$$\frac{\mu P_1 Q_1}{S P_m} = k_g \frac{\Delta P}{L}, \quad \ldots\ldots (8)$$

where P_m and ΔP are the mean pressure and pressure drop, respectively, given by

$$P_m = \frac{P_1 + P_2}{2} \quad \ldots\ldots (9)$$

and $\Delta P = P_1 - P_2$. $\ldots\ldots (10)$

In Eq. 8, k_g is the apparent gas permeability of the core given by

$$k_g = k_g^{(\infty)}\left(1 + \frac{b}{P_m}\right). \quad \ldots\ldots (11)$$

The two models in Eqs. 7 and 8 are further used below to determine k_g, $k_g^{(\infty)}$ and b from experimental data Q_1, P_1, and P_2. Moreover, to estimate the dependence of the Klinkenberg effect on S_w before and after polymer treatment, we use a dimensionless quantity, κ, defined by the ratio

$$\kappa = \frac{k_g^{(\mathrm{atm})} - k_g^{(\infty)}}{k_g^{(\infty)}} = \frac{b}{P_m^{(\mathrm{atm})}}, \quad \ldots\ldots (12)$$

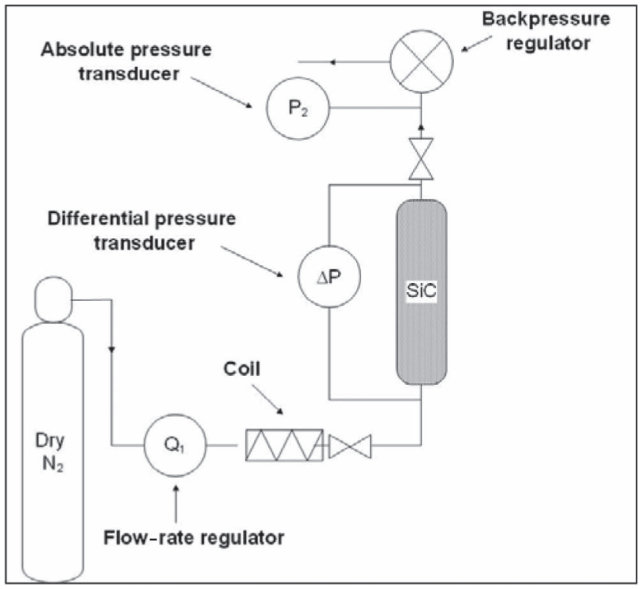

Fig. 2—Coreflood test equipment used to the study Klinkenberg effects.

where $k_g^{(atm)}$ is the apparent permeability to gas at mean pressure $P_m^{(atm)}$ close to the atmospheric pressure.

Coreflood Test Equipment and Procedure. The coreflood test equipment used to investigate the influence of polymer on the Klinkenberg effect is illustrated in **Fig. 2.** The porous medium was confined in a Pyrex* cylindrical cell ($L = 10$ cm, inner diameter $= 4$ cm) vertically oriented for all gas/water or water/gas displacements to avoid front instability resulting from density contrasts. Brine and dry gas were injected sequentially with a volumetric pump and a flow-rate regulator, respectively. Brine was injected from the bottom of the cell, while gas was injected from either the top or the bottom of the cell. Gas flow rate was controlled at the core inlet using a flow-rate regulator. Gas pressure drop was measured between core inlet and outlet with a differential pressure transducer. A backpressure regulator was placed at the core outlet for experiments to be performed at various mean pressures P_m in the core. The backpressure, P_2, was also measured with an absolute-pressure transducer.

Porosity and saturation were measured by mass balance and gamma ray attenuation. The different sequences of the experimental procedure are described below.

1. Core packing using a vibrating table
2. Gas-permeability measurement at different mean pressures, $k_g^{(1)}$, on the original dry core ($S_w = 0$); determination of intrinsic permeability, $k_g^{(\infty)(1)}$ and relative Klinkenberg effect $\kappa^{(1)}$
3. Brine saturation of the core after CO_2 flush
4. Measurement of porosity, $\phi^{(1)}$, and brine permeability, $k_w^{(1)}$, of the original core ($S_w = 1$)
5. Gas drainage until stationary brine saturation, $S_w^{(1)}$; measurement of local brine saturation along the core by gamma ray attenuation (initial state)
6. Measurement of the effective permeability to gas varying the outlet backpressure (i.e., varying P_m); determination of the corrected effective permeability to gas, $k_g^{(\infty)(1)}(S_w)$, and relative Klinkenberg effect, $\kappa^{(1)}(S_w)$; measurement of local brine saturation along the core by gamma ray attenuation (final state)
7. Repetition of Step 5 to vary stationary brine saturation value (a smaller brine saturation was obtained by increasing the gas flow rate to perform drainage in Step 5); repetition of Step 6
8. CO_2 flushing of the core followed by brine ([KI] = 10 g/L) injection until complete saturation of the core; CO_2 preflushing was performed to improve complete brine saturation during imbibition (this improvement is achieved owing to solubilization of CO_2 bubbles that otherwise would remain trapped if imbibition were performed on a nitrogen-saturated core)
9. Brine ([KI] = 5 g/L) injection to determine salt dispersion front, followed by an injection of 3 pore volumes of polymer solution; effluent viscosity is measured to quantify polymer adsorption
10. Injection of brine to displace the nonadsorbed polymer; this leads to a core called "treated core," on which brine permeability, $k_w^{(2)}$, is measured to estimate brine permeability reduction, R_{kw}
11. Gas drainage until stationary brine saturation, $S_w^{(2)}$; measurement of local brine saturation along the core by gamma ray attenuation
12. Measurement of the effective permeability to gas varying the outlet backpressure (i.e., varying P_m); determination of the corrected effective permeability to gas, $k_g^{(\infty)(2)}(S_w)$, and relative Klinkenberg effect, $\kappa^{(2)}(S_w)$; measurement of local brine saturation along the core by gamma ray attenuation
13. Repetition of Step 11 to vary stationary brine saturation value by varying gas drainage flow rate; repetition of Step 12; estimation of gas-permeability reduction, R_{kg}

Inertial Effects. ***Physical Model.*** When considering a classical Darcy experiment, one can observe a deviation from the linear dependence of pressure drop to mass flow rate when flow rate is sufficiently large. This is the result of significant inertial effects at the pore scale that can be taken into account macroscopically by correcting Darcy's law. For Reynolds numbers $\mathrm{Re} = \frac{\rho_1 Q_1 d_g}{S\mu}$ greater than roughly unity, it is now clear that inertia can be described by a quadratic velocity correction term as proposed initially by Forchheimer (1901). For ideal-gas and isothermal flow, this leads to the following 1D relationship integrated over the core length L:

$$\frac{P_1^2 - P_2^2}{2\mu P_1 \frac{Q_1}{S} L} = \frac{1}{k_{\mathrm{eff}}} + \beta \frac{M}{RT} \frac{P_1}{\mu} \frac{Q_1}{S}, \quad \ldots\ldots\ldots\ldots\ldots\ldots\ldots\ldots (13)$$

where, as before, M is the molar mass of gas, R is the ideal-gas constant, T is the temperature, and β is the inertial resistance coefficient.

In the inertial regime, our experiments were performed on relatively high-permeability cores (see results below) at relatively high mean pressure (caused by high flow rates). For these reasons, the Klinkenberg effect was negligible while studying inertial effects so that k_{eff} in Eq. 13 can be understood as $k_g^{(\infty)}$.

Several authors have shown that β depends strongly on physical properties of the porous medium (e.g., porosity, permeability, tortuosity) in a complex way, and it is beyond the scope of this work to derive a precise formalism on β. Provided that water is immobile within the medium, Geertsma (1974) proposed that β could be consistently correlated to the effective porosity and effective permeability according to

$$\beta = \frac{\lambda}{\phi_{\mathrm{eff}}^{5.5} k_{\mathrm{eff}}^{0.5}}, \quad \ldots\ldots\ldots\ldots\ldots\ldots\ldots\ldots\ldots\ldots\ldots\ldots\ldots\ldots (14)$$

where λ is constant and ϕ_{eff} and k_{eff} are respectively defined by

$$\phi_{\mathrm{eff}} = \phi(1 - S_w) \quad \ldots\ldots\ldots\ldots\ldots\ldots\ldots\ldots\ldots\ldots\ldots\ldots\ldots\ldots (15)$$

and $$k_{\mathrm{eff}} = k\, k_{rg}(S_w), \quad \ldots\ldots\ldots\ldots\ldots\ldots\ldots\ldots\ldots\ldots\ldots\ldots\ldots\ldots (16)$$

where k and $k_{rg}(S_w)$ are the intrinsic permeability and gas relative permeability at water saturation S_w. Eq. 14 is tested in the following section as a possible correlation for β.

Coreflood Test Equipment and Procedure. The coreflood test equipment used to study inertial effects is depicted in **Fig. 3.** The porous medium was confined in a stainless-steel cell ($L = 10$ cm, inner diameter $= 1$ cm, outer diameter $= 5$ cm) placed vertically to avoid preferential pathways caused by density contrasts. Gas and water were coinjected from the bottom of the cell at different flow rates so that different saturation values could be reached. Water

* Mark of Preciver, Maisons Alfort, France.

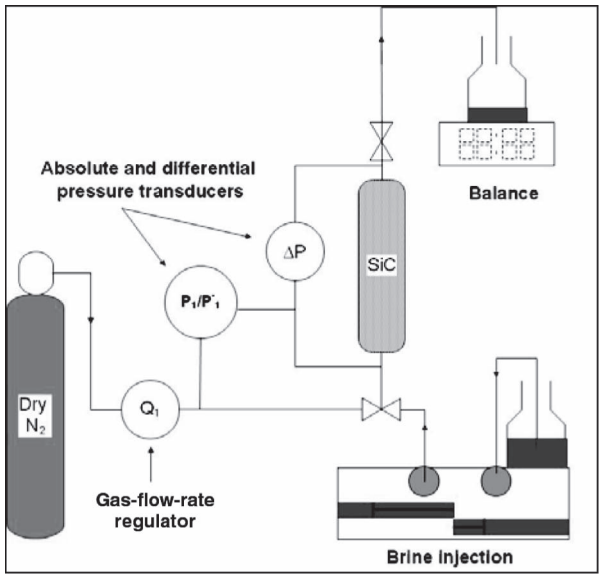

Fig. 3—Coreflood test equipment to study inertial effects.

was injected with a volumetric pump, while gas flow was controlled with a flow-rate regulator. Steady state was assumed when water production measured at the core outlet was equal to the inlet water flow rate. Pressure drop was measured between two pressure taps placed along the core at 3 cm from the inlet and outlet, respectively. Because flow is in the inertial regime, capillary pressure is assumed to be negligible, and the measured pressure drop is supposed to be that in the gas phase. Absolute pressure was also measured at the core inlet, and the saturation was measured by weighting.

The experimental protocol is described below.

1. Core packing
2. Gas-permeability measurement, $k_g^{(1)}$, and inertial resistance coefficient, $\beta^{(1)}$, on the original dry core ($S_w = 0$)
3. Brine saturation of the core after CO_2 flush
4. Measurement of porosity, ϕ, and brine permeability of the original core, $k_w^{(1)}$
5. Coinjection of gas and brine until stationary brine saturation, $S_w^{(1)}$; measurement of effective permeability to gas, $k_{\text{eff}}^{(1)}(S_w)$, and inertial resistance coefficient, $\beta^{(1)}(S_w)$ (this step was repeated for different brine saturations obtained by varying water-to-gas flow-rate ratio)
6. CO_2 flushing of the core followed by brine ([KI] = 10 g/L) injection until complete saturation of the core; here again, CO_2 was used to improve brine saturation as described in the *Coreflood Test Equipment and Procedure* section of Klinkenberg effects (Step 8)
7. Brine ([KI] = 5 g/L) injection, to determine salt dispersion front, followed by an injection of 3 pore volumes of polymer solution; effluent viscosity is measured to quantify polymer adsorption
8. Injection of brine to displace the nonadsorbed polymer; this leads to a core state called "treated core," on which brine permeability, $k_w^{(2)}$, is measured to estimate brine permeability reduction, R_{kw}
9. Coinjection of gas and brine until stationary brine saturation, $S_w^{(2)}$; measurement of effective permeability to gas, $k_{\text{eff}}^{(2)}(S_w)$ and inertial resistance coefficient, $\beta^{(2)}(S_w)$ on the treated core (this step was repeated for different brine saturations)

Results

Polymer Adsorption. The polymer front delay with respect to the salt dispersion front is caused by an adsorption mechanism. In the absence of a significant excluded pore volume, as is the case with the model granular packs used here, this delay can be interpreted to estimate the amount of adsorbed polymer (Barreau 1996). Using this technique, we find an adsorption corresponding to 115 $\mu g.g^{-1}$ for the granular pack made from SiC 50-μm grain diameter, while it is 90 $\mu g.g^{-1}$ for the one made from SiC 30-μm grain diameter.

TABLE 1—PHYSICAL PROPERTIES AND PERMEABILITY REDUCTIONS OF THE TWO SiC 30-μm CORES PREPARED TO STUDY THE KLINKENBERG EFFECT

	SiC 30 μm		SiC 50 μm	
	Original	Treated	Original	Treated
ϕ (Core 1)	0.42	–	0.41	–
k_w (m^2) (Core 1)	4.8×10^{-13}	–	1.5×10^{-12}	–
ϕ (Core 2)	0.44	–	–	–
k_w (m^2) (Core 2)	5.5×10^{-13}	–	–	–
S_w	0.34	0.52	–	–
R_{kw}	2.8		1.2	
R_{kg}	1.4		1	

Stationary Brine Saturation. Experimental results given in **Table 1** show a significant increase in stationary brine saturation after polymer adsorption. This is in accordance with observations on water/oil systems and is a direct consequence of brine retention in the hydrosoluble adsorbed polymer, in addition to capillary trapping phenomena in small pores.

Permeability Reduction. Results on permeability reduction to water and gas, as defined by Eq. 1, are given in Table 1.

Reduction of water permeability varies from 1.2 to 2.8 for the two different types of cores ($d_g = 30$ μm and $d_g = 50$ μm) and is always larger than the gas-permeability reduction, which remains close to 1. This illustrates and confirms the DPR effect of polymer for gas/water flow. These results are consistent with the wall effect hypothesis.

Klinkenberg Effects. Two different cores, referred to as Core 1 and Core 2, were prepared with SiC powder having a mean grain size of $d_g = 30$ μm to study the Klinkenberg effect. Porosity and intrinsic permeability of these two cores are reported in Table 1, indicating a very good reproducibility of the packing procedure. Examples of gas-flow experimental results obtained on Core 1 at $S_w^{(1)} = 0$, $S_w^{(1)} = 0.12$, and $S_w^{(1)} = 0.34$ before polymer treatment are reported in **Figs. 4 and 5.** These two figures clearly show, in accordance with Eqs. 7 and 8, that k_g can be determined precisely in a graph of $\frac{\mu P_1 Q_1}{S P_m}$ vs. $\Delta P/L$, while $k_g^{(\infty)}$ and b are obtained using the representation $\frac{\mu L Q_1 P_1}{S \Delta P}$ vs. P_m with an excellent precision. As expected, $k_g^{(\infty)(1)}$ decreases as $S_w^{(1)}$ increases. All the results on $S_w^{(1)}$, $k_g^{(\text{atm})(1)}$, $k_g^{(\infty)(1)}$, and $\kappa^{(1)}$ obtained on the two cores for all the saturation values are reported in **Table 2.** In **Fig. 6,** we have represented the evolution of $\kappa^{(1)}$ (see Eq. 12) vs. S_w. This figure

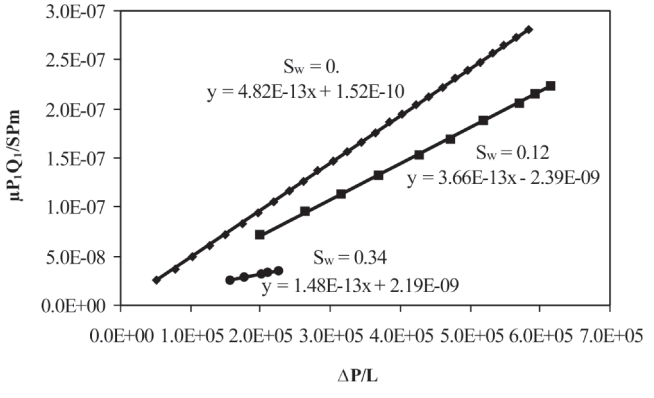

Fig. 4—Determination of k_g (see Eq. 8) for three values of water saturation before polymer injection.

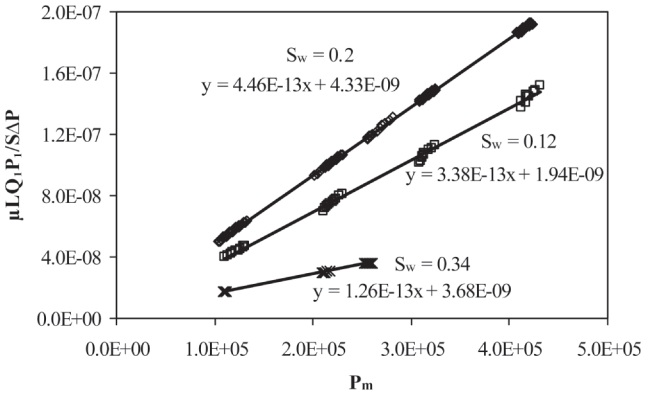

Fig. 5—A $\frac{\mu L Q_1 P_1}{S \Delta P}$ vs. P_m graph allowing the estimation of $k_g^{(\infty)}$ and b (see Eq. 7). Experimental results obtained at $S_w^{(1)}$=0, $S_w^{(1)}$=0.12, and $S_w^{(1)}$=0.34 before polymer treatment on Core 1.

shows a very good reproducibility of gas-flow experiments and two distinct regions in the evolution of $\kappa^{(1)}$, with S_w separated by a crossover at $S_w^{(1)} \approx 0.2$. At low saturation values, the Klinkenberg effect remains constant, while above the crossover value, $\kappa^{(1)}$ seems to increase linearly with $S_w{}^{(1)}$: $\kappa^{(1)} \approx 8\%$ for $S_w{}^{(1)} < 0.2$ and increases to approximately 17% at $S_w{}^{(1)} = 0.34$. Many physical origins can be put forth (see discussion below), the most probable one being a microscopic water distribution that may be very different at the pore scale while $S_w{}^{(1)}$ varies. In our experiments, we were only able to check that the local saturation field along the core was not significantly modified during gas injection performed to measure $k_g^{(\infty)}$ and b. This is shown in **Fig. 7,** where we have reported two initial (end of Step 5 of the experimental protocol) and final (end of Step 6 of the protocol) local saturations along the core ($S_w{}^{(1)} = 0.12$ and $S_w{}^{(1)} = 0.34$). These saturation profiles present a significant gradient and an "end effect," especially for the larger value of S_w. Clearly, more-detailed information would be necessary at a smaller (pore) scale to understand the evolution of κ with S_w.

As indicated in the protocol, injection of gas was repeated on Core 2 after polymer treatment. Because stationary saturation is difficult to control a priori, $k_g^{(\mathrm{atm})(2)}$, $k_g^{(\infty)(2)}$, and $b^{(2)}$ were measured at saturation slightly different from those in the absence of adsorbed polymer (namely, at $S_w{}^{(2)} = 0.18$ and $S_w{}^{(2)} = 0.35$) and are reported in Table 2. The corresponding values of $\kappa^{(2)}$ indicated in Table 2 are represented in Fig. 6. One can clearly see on this figure that κ is reduced drastically after polymer has been injected because the Klinkenberg effect fades away after treatment ($\kappa^{(2)} < 0.7\%$ at $S_w{}^{(2)} = 0.35$, and $\kappa^{(2)} \approx 1\%$ at $S_w{}^{(2)} = 0.18$). This result can be explained qualitatively by the fact that water distribution is

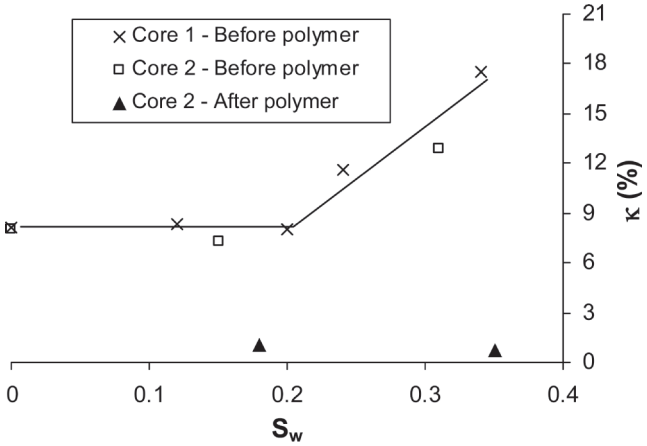

Fig. 6—Evolution of κ with S_w before and after polymer; Core 1 and 2 of SiC 30 μm.

TABLE 2—EFFECTIVE PERMEABILITIES TO GAS AND κ AT DIFFERENT SATURATIONS OBTAINED ON THE TWO SiC 30-μm CORES (1) BEFORE AND (2) AFTER POLYMER TREATMENT

S_w	$k_g^{(\mathrm{atm})}$ (m^2)	$k_g(\infty)$ (m^2)	κ(%)
0 (Core 1) (1)	4.82×10^{-13}	4.46×10^{-13}	8.1
0.12 (Core 1) (1)	3.66×10^{-13}	3.38×10^{-13}	8.3
0.20 (Core 1) (1)	2.15×10^{-13}	1.99×10^{-13}	8.0
0.24 (Core 1) (1)	1.64×10^{-13}	1.47×10^{-13}	11.6
0.34 (Core 1) (1)	1.48×10^{-13}	1.26×10^{-13}	17.5
0 (Core 2) (1)	5.40×10^{-13}	5.00×10^{-13}	8
0.15 (Core 2) (1)	2.79×10^{-13}	2.60×10^{-13}	7.3
0.31 (Core 2) (1)	2.10×10^{-13}	1.86×10^{-13}	12.9
0.18 (Core 2) (2)	2.92×10^{-13}	2.89×10^{-13}	1.04
0.35 (Core 2) (2)	1.45×10^{-13}	1.44×10^{-13}	0.69

modified by the presence of the adsorbed polymer at the pore scale, in addition to the fact that gas/water interface is also modified (see details in the Discussion section below). Again, further microscale investigations would be necessary to have more physical quantitative insights into this phenomenon.

Inertial Effects. In this series of experiments, we used a core made from SiC powder having a mean grain size of $d_g = 50$ μm. An example of experimental results obtained over a wide range of the Reynolds number on this type of core is reported in **Fig. 8,** where we have represented $\frac{S}{2\mu L}\frac{(P_1^2 - P_2^2)}{P_1}$ vs. Q_1 in a Darcy plot. This figure clearly shows the inertial effect for Re>2. The same results represented in a Forchheimer plot in **Fig. 9** [i.e., $Y = (P_1^2 - P_2^2)S/(2\mu P_1 Q_1 L)$ vs. $X = MP_1Q_1/(RT\mu S)$; see Eq. 13] for Re>2 confirms that beyond this value of the Reynolds number, the correction is quadratic, and the model in Eq. 13 is valid. Using this last representation allows the determination of the inertial resistance coefficient (slope of the curve) as well as an estimation of the effective gas permeability (intercept point). Note, however, that this method leads to an overestimation of the effective permeability.

Different stationary water saturation fields were obtained before polymer injection using a water/gas coinjection technique as described above. Gas permeabilities and inertial resistance coefficients were determined for all the water saturations that were obtained ($S_w{}^{(1)} = 0.23$, $S_w{}^{(1)} = 0.29$, and $S_w{}^{(1)} = 0.35$). The corresponding experimental data are reported in Table 3 and represented in **Fig. 10** (Darcy plot) and **Fig. 11** (Forchheimer plot). As expected, these results indicate that gas permeability decreases and that the inertial resistance coefficient increases when water satu-

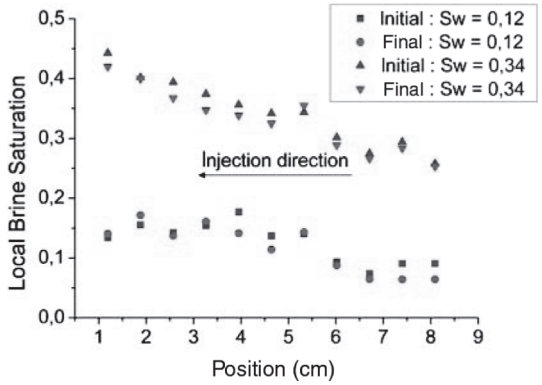

Fig. 7—Local brine saturation before polymer treatment vs. position along Core 1 of SiC 30 μm; S_w=0.12 and 0.34.

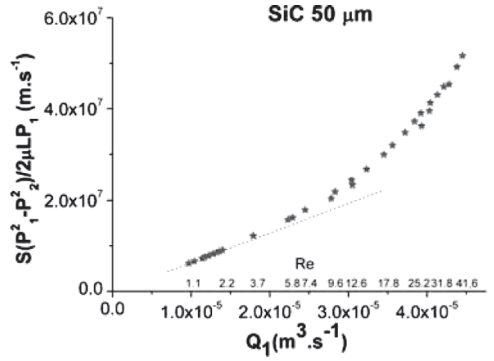

Fig. 8—Darcy plot of experimental data obtained on dry core of SiC 50 µm.

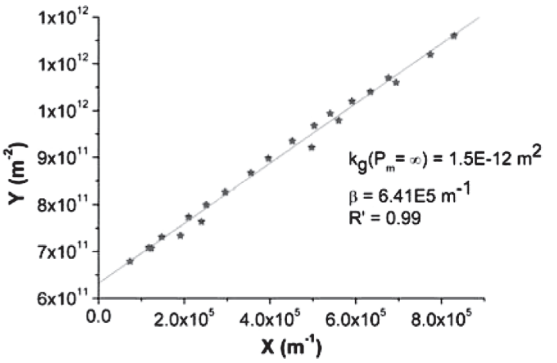

Fig. 9—Forchheimer plot of experimental data obtained on dry core of SiC 50 µm.

ration increases. Moreover, as shown in **Fig. 12,** β seems to be well correlated to ϕ_{eff} and k_{eff}, according to the relationship in Eq. 14.

Gas/water coinjection was repeated on the same core after polymer injection, as indicated in the experimental protocol. Again, because the stationary saturation could not be controlled a priori, results are available at water saturations different from those before polymer treatment [i.e., $S_w^{(2)} = 0.17$, $S_w^{(2)} = 0.27$, and $S_w^{(2)} = 0.32$; see **Table 3**]. The corresponding experimental results are reported in **Fig. 13** (Darcy plot) and **Fig. 14** (Forchheimer plot). After polymer treatment, the same behavior is observed on the dependence of $k_{\text{eff}}^{(2)}$ and $\beta^{(2)}$ on the water saturation. However, an important result lies in the reduction of the inertial resistance coefficient after polymer injection. In fact, as shown in **Fig. 15,** where we have reported experimental data obtained on the original and treated core for very close water-saturation values, the equivalent pressure drop (corrected from compressibility effects), keeping Q_1 constant, is reduced significantly when polymer is present. This result is confirmed in **Fig. 16,** where we have represented β vs. $\phi_{\text{eff}}^{-5.5}\, k_{\text{eff}}^{-0.5}$, both before and after polymer treatment. First, it can be seen that the correlation in Eq. 14 remains consistent after polymer treatment on the range of the effective properties investigated here. Second, for a given set of the effective properties, the inertial resistance coefficient is smaller after polymer adsorption in the core in comparison to that on the original core. This observation confirms a similar trend obtained on sandstones cores (Elmkies et al. 2002). This mechanism could have practical consequences of great interest, considering head losses close to the wellbore after polymer treatment of a gas well.

Discussion

In this section, we shall briefly discuss some plausible physical phenomena that may explain some of the observations reported above. It should be noticed, however, that these observations are macroscopic results at the core scale, requiring more thorough pore-scale investigation to get insight into their detailed physical explanation. One key point in particular is the fluid distribution within the pores and its dependence upon saturation, flow rate, and the presence or absence of adsorbed polymer. Results on the DPR observed here are consistent with previous results (Zaitoun and Kohler 1989) and might be explained by the same mechanisms as those presented in the Introduction section of this paper.

The global increase of the Klinkenberg effect with the saturation in the absence of polymer is coherent with the fact that this effect increases when the effective pore diameter opened to gas flow decreases. It is also in agreement with some previous observations (Li and Horne 2004), although in contradiction with others (Sampath and Keighin 1982). The existence of a water-saturation crossover value, below which this effect remains almost constant and above which it increases quasilinearly with S_w, might be explained by the distribution of the (immobile) water phase within the pore network. In fact, one might expect that below this crossover value of S_w, water is trapped under the form of pendular rings that do not contribute significantly to the pore reduction, leaving the Klinkenberg effect quasi-unaffected in comparison to the dry porous medium ($S_w = 0$). Above this value, one can expect a funicular distribution of (immobile) water corresponding to pendular rings connected by wetting films covering solid grains. In this situation, water films would contribute to a significant pore reduction yielding an increase of the Klinkenberg effect.

The drastic reduction of the Klinkenberg effect after polymer adsorption might be explained by the fact that the smaller pore throats are clogged up because of the presence of the adsorbed polymer layer so that gas flow occurs in larger channels, leading to a net reduction of the Klinkenberg effect in comparison to a polymer-free configuration. More subtle effects of gas/polymer interfacial interaction might also be part of this explanation.

In the inertial regime, an increase of the inertial resistance coefficient β with the water saturation observed in our experiments

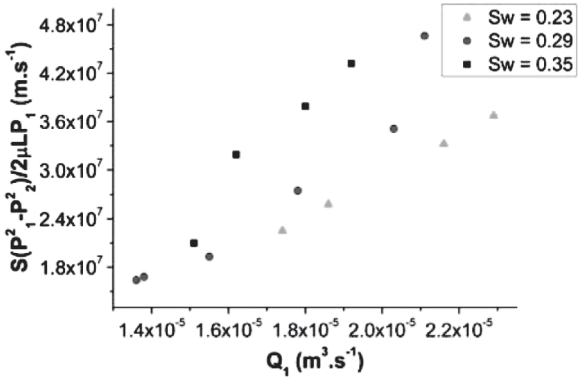

Fig. 10—Darcy plot of experimental data obtained before polymer on core of SiC 50 µm partially saturated; S_w varies between 0.23 and 0.35.

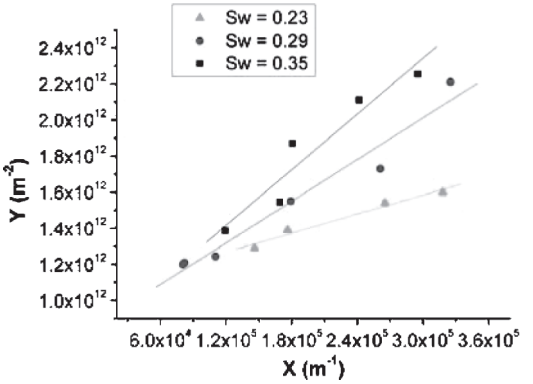

Fig. 11—Forchheimer plot of experimental data obtained before polymer on core of SiC 50 µm partially saturated; S_w varies between 0.23 and 0.35.

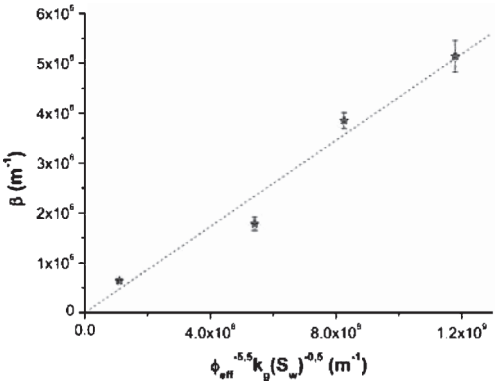

Fig. 12—Inertial resistance coefficient on core of SiC 50 μm before polymer vs. $\phi_{eff}^{-5.5}\ k_{eff}^{-0.5}$.

in the absence of polymer is consistent with previous observations (Li and Engler 2001). In essence, this is a direct consequence of reducing the gas effective permeability while increasing the (immobile) water saturation. This is in accordance with extensive results available for one-phase flow in porous media (Edwards et al. 1990). It is confirmed by the dependence of β with ϕ_{eff} and k_{eff} obtained from our experiments, which is in good agreement with the correlation proposed by Geertsma (1974) (see Eq. 14).

In the presence of polymer, the major result is a clear reduction of the inertial resistance coefficient in comparison to the case without adsorbed polymer. A possible explanation of this behavior lies in the smoothing effect of the adsorbed polymer layer, reducing roughness and tortuosity of gas flow paths.

From a practical point of view, this last result opens an interesting perspective for field applications. Beyond the DPR effect, polymer adsorption would allow a reduction of inertial effects. The reduction of this (unwanted) extra friction can be of major concern in the domain of gas storage during the injection process, as well as during production periods, allowing larger flow rates at the same bottomhole pressure.

Conclusions

In this work, the impact of polymer adsorption in porous media on gas flow in both the Klinkenberg and inertial regimes was investigated experimentally with and without the presence of a stationary water saturation. Our experiments performed on model SiC granular packs led to the following conclusions.

1. DPR resulting from nonionic polyacrylamide adsorption is confirmed in this type of unconsolidated core for gas/water flow. Permeability to gas is not markedly modified, while permeability to water is significantly reduced.
2. Before polymer injection, and in the presence of a stationary water saturation S_w, the Klinkenberg effect exhibits two distinct behaviors separated by a crossover saturation. While this effect remains constant for S_w smaller than the crossover value, it increases linearly with S_w beyond the crossover.
3. After polymer adsorption, the Klinkenberg effect is strongly decreased.
4. In accordance with previous works, inertial effects are increased significantly by the presence of water saturation. For the granular pack models used in this work, a correlation between the inertial resistance coefficient, β, and $\phi_{eff}^{-5.5}k_{eff}^{-0.5}$, as proposed elsewhere (Geertsma 1974), was found consistent.
5. The presence of polymer leads to a reduction of the inertial resistance coefficient. The rate of increase of β with $\phi_{eff}^{-5.5}k_{eff}^{-0.5}$ is significantly smaller after polymer, yet this effect is in competition with the increase of stationary brine saturation, which increases β and is induced by polymer adsorption.

TABLE 3—EFFECTIVE PERMEABILITIES TO GAS, INERTIAL RESISTANCE COEFFICIENT, AND EFFECTIVE POROSITY OBTAINED ON ORIGINAL AND TREATED SiC 50-μm CORE (1) BEFORE AND (2) AFTER POLYMER TREATMENT

S_w	$k_g(S_w)$ (m^2)	β (m^{-1})	ϕ_{eff}
0 (1)	1.5×10^{-12}	6.4×10^5	0.41
0.23 (1)	9.5×10^{-13}	1.8×10^6	0.32
0.29 (1)	1.2×10^{-12}	3.9×10^6	0.29
0.35 (1)	1.3×10^{-12}	4.7×10^6	0.27
0.17 (2)	1.1×10^{-12}	1.1×10^6	0.34
0.27 (2)	9.9×10^{-13}	1.9×10^6	0.30
0.32 (2)	8.5×10^{-13}	2.3×10^6	0.29

Nomenclature

b = Klinkenberg constant (Pa)
d_g = mean grain size (m)
k = permeability (m^2)
L = core length (m)
P = pressure (Pa)
P_m = arithmetic mean pressure (Pa)
Q = volume flow rate (m^3.s^{-1})
R_{kg} = gas-permeability reduction
R_{kw} = brine-permeability reduction
S = core section (m^2)
S_w = brine saturation
T = temperature (K)
β = inertial resistance coefficient (m^{-1})
μ = gas dynamic viscosity (Pa·s)
ρ = density (kg.m^{-3})
κ = Klinkenberg effect

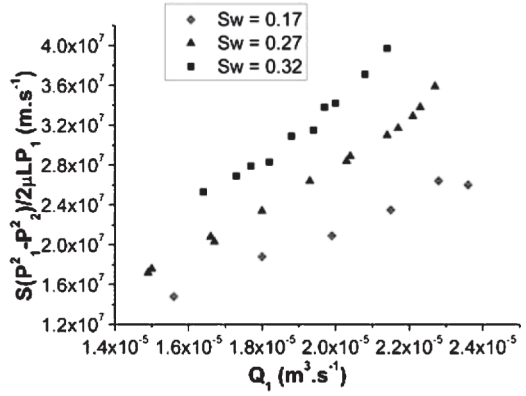

Fig. 13—Darcy plot of experimental data obtained on partially saturated core of SiC 50 μm after polymer. S_w varies between 0.17 and 0.32.

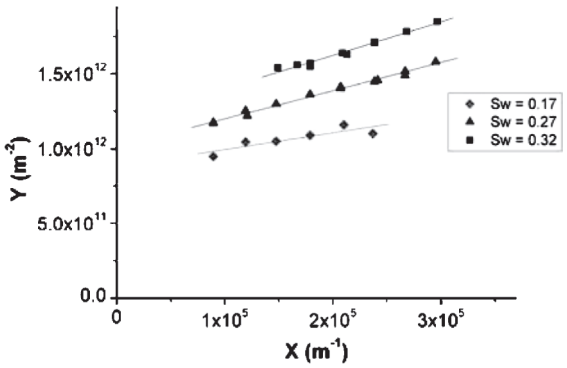

Fig. 14—Forchheimer plot of experimental data obtained on partially saturated core of SiC 50 μm after polymer. S_w varies between 0.17 and 0.32.

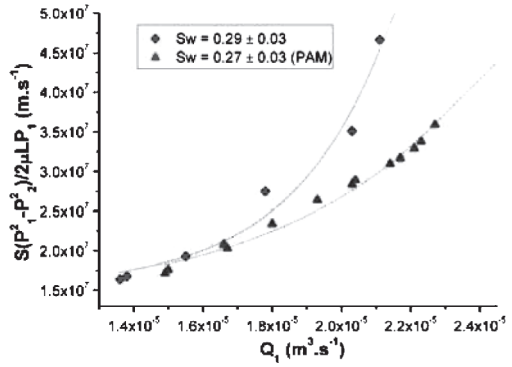

Fig. 15—Darcy plot of experimental data obtained on partially saturated core of SiC 50 µm before polymer (S_w=0.27) and after polymer (S_w=0.29).

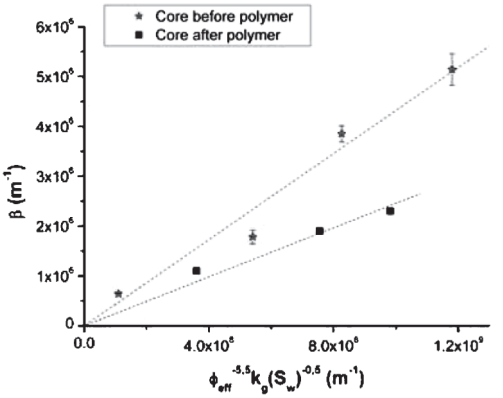

Fig. 16—Inertial resistance coefficient on core of SiC 50 µm before and after polymer vs. $\phi_{eff}^{-5.5}\ k_{eff}^{-0.5}$.

Subscripts

1, 2 = core inlet, outlet
eff = effective
g = gas phase
w = water phase

Superscripts

(1) = original core
(2) = treated core

Acknowledgments

Financial support from the Institut Français du Pétrole and Gaz de France is gratefully acknowledged. Special thanks are due to N. Blin for his help in performing some of the experiments presented in this work.

References

Barreau, P. 1996. Modifications des propriétés polyphasiques d'un milieu poreux en présence d'une couche de polymère adsorbé : études expérimentale et numérique. PhD thesis, Ecole Nationale Supérieure d'Arts et Métiers, Bordeaux, France.

Barreau, P., Lasseux, D., Bertin, H., Glénat, Ph., and Zaitoun, A. 1997. Polymer Adsorption Effect on Relative Permeability and Capillary Pressure: Investigation of a Pore Scale Scenario. Paper SPE 37303 presented at the SPE International Symposium on Oilfield Chemistry, Houston, 18–21 February. DOI: 10.2118/37303-MS.

Broseta, D., Medjahed, F., Lecourtier, J., and Robin, M. 1995. Polymer Adsorption/Retention in Porous Media: Effects of Core Wettability and Residual Oil. *SPE Advanced Technology Series* **3** (1): 103–112. SPE-24149-PA. DOI: 10.2118/24149-PA.

Chauveteau, G., Nabzar, L., El Attar, Y., and Jacquin, C. 1996. Pore Structure and Hydrodynamics in Sandstones. Paper SCA 9607 presented at the Intl. Symposium of the Soc. of Core Analysts, Montpellier, France, 8–10 September.

Dawe, R.A. and Zhang, U. 1994. Mechanistic study of the selective action of oil and water penetrating into a gel emplaced in a porous medium. *J. Pet. Sci. & Eng.* **12** (2): 113–125. DOI: 10.1016/0920-4105(94)90011-6.

Edwards, D.A., Shapiro, M., Bar-Yoseph, P., and Shapira, M. 1990. The influence of Reynolds number upon the apparent permeability of spatially periodic arrays of cylinders. *Physics of Fluids* **2** (1)**:** 45–55.

Elmkies, Ph., Lasseux, D., Bertin, H., Pichery, T., and Zaitoun, A. 2002. Polymer Effect on Gas/Water Flow in Porous Media. Paper SPE 75160 presented at the SPE/DOE Symposium on Improved Oil Recovery, Tulsa, 13–17 April. DOI: 10.2118/75160-MS.

Forchheimer, P. 1901. Wasserbewegung durch boden. *Z. Ver. Deutsch Ing.* **45:** 1782–1788.

Geertsma, J. 1974. Estimating the Coefficient of Inertial Resistance in Fluid Flow Through Porous Media. *SPEJ* **14** (5): 445–450. SPE-4706-PA. DOI: 10.2118/4706-PA.

Klinkenberg, L.J. 1941. The permeability of porous media to liquids and gases. *Drilling and Production Practice,* 200–213. New York City: American Petroleum Inst.

Li, D. and Engler, T.W. 2001. Literature Review on Correlations of the Non-Darcy Coefficient. Paper SPE 70015 presented at the SPE Permian Basin Oil and Gas Recovery Conference, Midland, Texas, 15–17 May. DOI: 10.2118/70015-MS.

Li, K. and Horne, R.N. 2004. Experimental Study of Gas Slippage in Two-Phase Flow. *SPEREE* **7** (6): 409–415. SPE-89038-PA. DOI: 10.2118/89038-PA.

Liang, J. and Seright, R.S. 2000. Wall-Effect/Gel-Droplet Model of Disproportionate Permeability Reduction. Paper SPE 59344 presented at the SPE/DOE Improved Oil Recovery Symposium, Tulsa, 3–5 April. DOI: 10.2118/59344-MS.

Médout-Marère, V., El Ghzaoui, A., Charnay, C., Douillard, J.M., Chauveteau, G., and Partyka, S. 2000. Surface Heterogeneity of Passively Oxidized Silicon Carbide Particles: Hydrophobic-Hydrophilic Partition. *J. Colloid Interface Sci.* **223** (2): 205–214. DOI: 10.1006/jcis.1999.6625.

Mennella, A., Chiappa, L., Bryant, S.L., and Burrafato, G. 1998. Pore-Scale Mechanism for Selective Permeability Reduction by Polymer Injection. Paper SPE 39634 presented at the SPE/DOE Improved Oil Recovery Symposium, Tulsa, 19–22 April. DOI: 10.2118/39634-MS.

Nicholls, C.I. and Heaviside, J. 1988. Gamma-Ray-Absorption Techniques Improve Analysis of Core Displacement Tests. *SPEFE* **1** (4): 69–75; *Trans.,* AIME, **285.** SPE 14421-PA. DOI: 10.2118/14421-PA.

Nilsson, S., Stavland, A., and Jonsbraten, H.C. 1998. Mechanistic study of disproportionate permeability reduction. Paper SPE 39635 presented at the SPE/DOE Improved Oil Recovery Symposium, Tulsa, 19–22 April. DOI: 10.2118/39635-MS.

Sampath, D. and Keighin, C.W. 1982. Factors Affecting Gas Slippage in Tight Sandstones of Cretaceous Age in the Uinta Basin. *JPT* **34** (11): 2715–2720. SPE-9872-PA. DOI: 10.2118/9872-PA.

Schneider, F.N. and Owens, W.W. 1982. Steady-State Measurements of Relative Permeability for Polymer/Oil Systems. *SPEJ* **22** (1): 79–86. SPE-9408-PA. DOI: 10.2118/9408-PA.

Sparlin, D.D. and Hagen, R.W. Jr. 1984. Controlling water in producing operations. *World Oil* **205** (6): 137–142.

White, J.L., Goddard, J.E., and Phillips, H.M. 1973. Use of Polymers to Control Water Production in Oil Wells. *JPT* **25** (2): 143–150. SPE-3672-PA. DOI: 10.2118/3672-PA.

Zaitoun, A. and Kohler, N. 1988. Two-Phase Flow Through Porous Media: Effect of an Adsorbed Polymer Layer. Paper SPE 18085 presented at the SPE Annual Technical Conference and Exhibition, Houston, 2–5 October. DOI: 10.2118/18085-MS.

Zaitoun, A. and Kohler, N. 1989. Modification of water/oil and water/gas relative permeabilities after polymer treatment of oil or gas wells. *In Situ* **13** (1 and 2): 55–77.

Zaitoun, A. and Kohler, N. 2000. Production Well Water Shut-Off Treatments by Weak Polymer Gels. In *Novelties in Enhanced Oil and Gas Recovery, Progress in Mining and Oilfield Chemistry,* ed. I. Lakatos, **2:** 101–116. Budapest: Akademiai Kiado.

Zaitoun, A., Bertin, H., and Lasseux, D. 1998. Two-Phase Flow Property Modification by Polymer Adsorption. Paper SPE 39631 presented at the SPE/DOE Improved Oil Recovery Symposium Tulsa, 19–22 April. DOI: 10.2118/39631-MS.

Zaitoun, A., Kohler, N. and Guerrini, Y. 1991. Improved Polyacrylamide Treatments for Water Control in Producing Wells. *JPT* **43** (7): 862–867. SPE-18501-PA. DOI: 10.2118/18501-PA.

SI Metric Conversion Factors

atm	× 1.013 250*	E+05	= Pa
ft	× 3.048*	E–01	= m
ft^2	× 9.290 304*	E–02	= m^2
ft^3	× 2.831 685	E–02	= m^3
°F	(°F–32)/1.8		= °C
in.	× 2.54*	E+00	= cm

*Conversion factor is exact.

Vincent Blanchard was a PhD student at the University of Bordeaux and is currently at Forintek in Canada. His background is in polymer science. **Didier Lasseux** is a CNRS researcher at the University of Bordeaux (France). His expertise is on multiphase fluid mechanics in porous media applied to petroleum engineering (enhanced oil recovery) and many issues within industrial porous media. **Henri Bertin** is a CNRS researcher at the University of Bordeaux (France). His research interests are in fluid mechanics in porous media with application in petroleum engineering (EOR) and environment. **Thierry Pichery** is Project Leader at the Gaz de France Department of Exploration and Production (St. Denis, France), where he is the expert in well technology. **Guy Chauveteau,** now retired, was Senior Research Engineer at the Institut Français du Pétrole (IFP). His expertise is in flow in porous media, EOR, and polymer rheology. **René Tabary** is a senior research engineer in the Reservoir Engineering Department at the Exploration and Production Business Unit of IFP. He is the Project Leader of the Joint Industry Project "STARGEL," dedicated to new IFP microgel technology for water shutoff and conformance control, and he is also responsible for developing and evaluating EOR chemical flood processes at IFP. **Alain Zaitoun** has been Senior Research Engineer at IFP since 1980 and Project Leader in Well Productivity and Injectivity since 2002. His main expertise is in the area of polymer improved oil recovery processes. He is the author or coauthor of more than 20 technical papers and is a member of the SPE Oilfield Chemistry Symposium Committee.